Article

Cell Reports

Desynchronizing Embryonic Cell Division Waves Reveals the Robustness of *Xenopus laevis* Development

Graphical Abstract

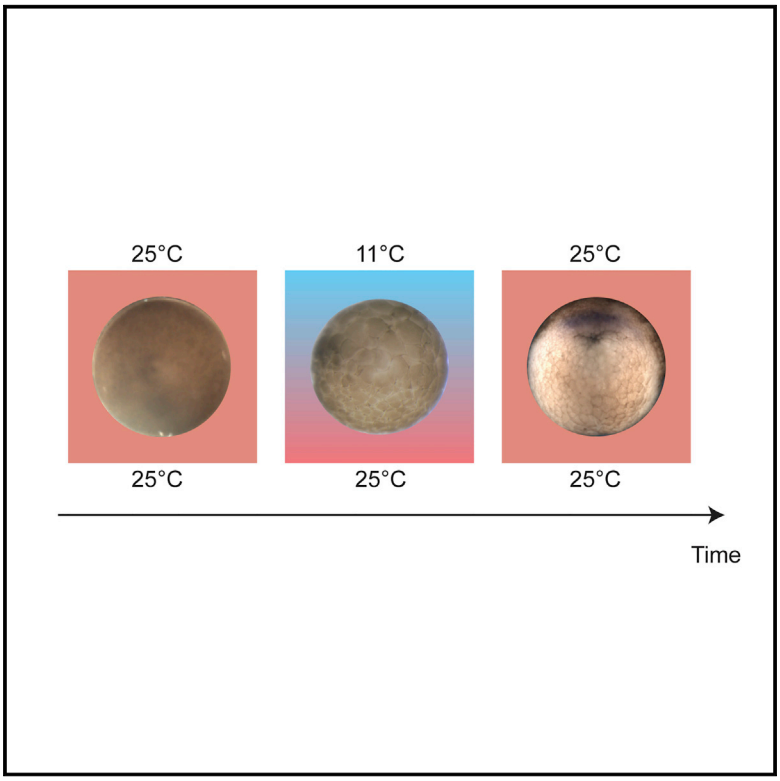

Authors

Graham A. Anderson, Lendert Gelens, Julie C. Baker, James E. Ferrell, Jr.

Correspondence

lendert.gelens@kuleuven.be (L.G.), james.ferrell@stanford.edu (J.E.F.)

In Brief

Anderson et al. apply strong temperature differences across young frog embryos to desynchronize the regular cell division timing. They find that all cells behave as independent oscillators. Moreover, they see that, although mesoderm induction becomes abnormal initially, the embryos are still able to get their development back on track.

Highlights

- Embryonic cell division waves are not caused by spatial cell-cell coupling
- Cell division waves gradually build up as a result of intrinsic period differences
- Desynchronizing the early divisions leads to mesoderm marker misexpression
- Mesoderm misexpression is corrected during involution, leading to viable embryos

Anderson et al., 2017, Cell Reports *21*, 37–46
October 3, 2017 © 2017 The Author(s).
https://doi.org/10.1016/j.celrep.2017.09.017

Cell Reports
Article

OPEN ACCESS
CellPress

Desynchronizing Embryonic Cell Division Waves Reveals the Robustness of *Xenopus laevis* Development

Graham A. Anderson,[1,6] Lendert Gelens,[1,2,3,6,*] Julie C. Baker,[4] and James E. Ferrell, Jr.[1,5,7,*]
[1]Department of Chemical and Systems Biology, Stanford University School of Medicine, Stanford, CA 94305-5174, USA
[2]Laboratory of Dynamics in Biological Systems, KU Leuven, Department of Cellular and Molecular Medicine, University of Leuven, 3000 Leuven, Belgium
[3]Applied Physics Research Group, Vrije Universiteit Brussel (VUB), 1050 Brussels, Belgium
[4]Department of Genetics, Stanford University School of Medicine, Stanford, CA 94305-5120, USA
[5]Department of Biochemistry, Stanford University School of Medicine, Stanford, CA 94305-5307, USA
[6]These authors contributed equally
[7]Lead Contact
*Correspondence: lendert.gelens@kuleuven.be (L.G.), james.ferrell@stanford.edu (J.E.F.)
https://doi.org/10.1016/j.celrep.2017.09.017

SUMMARY

The early *Xenopus laevis* embryo is replete with dynamic spatial waves. One such wave, the cell division wave, emerges from the collective cell division timing of first tens and later hundreds of cells throughout the embryo. Here, we show that cell division waves do not propagate between neighboring cells and do not rely on cell-to-cell coupling to maintain their division timing. Instead, intrinsic variation in division period autonomously and gradually builds these striking patterns of cell division. Disrupting this pattern of division by placing embryos in a temperature gradient resulted in highly asynchronous entry to the midblastula transition and misexpression of the mesodermal marker *Xbra*. Remarkably, this gene expression defect is corrected during involution, resulting in delayed yet normal *Xbra* expression and viable embryos. This implies the existence of a previously unknown mechanism for normalizing mesodermal gene expression during involution.

INTRODUCTION

The frog *Xenopus laevis* must solve a common problem after fertilization: how does a single, large (1.2 mm diameter) cell become thousands of somatic-sized cells that are ready to perform gastrulation and form an adult animal? Diverse animal embryos have found similar solutions to this problem. Zebrafish, *Drosophila*, and some species of frog all undergo multiple rounds of extremely rapid cleavages following fertilization (Keller et al., 2008; Olivier et al., 2010; Tomer et al., 2012; Movies S1 and S2). The first cell division arrives around 95 min post-fertilization (mpf) at 18°C, and regular rounds of cell divisions follow roughly every 35 min thereafter. At first, these divisions occur approximately synchronously in all cells in the embryo, but by division 5 and 6, a spatial wave of division is visible, with rounds of cell divisions progressing from one side of the embryo to the other (Boterenbrood et al., 1983). Zebrafish and *Drosophila* embryos likewise display waves of cell division (Tomer et al., 2012; Keller et al., 2008), suggesting that cell division waves may play a conserved role in early embryogenesis.

Cell division waves are not the only spatial waves in the early frog embryo (Ubbels et al., 1983). Within minutes after fertilization, a wave of intracellular calcium spreads from the sperm entry point across the egg (Figure 1), and it contributes to the block to polyspermy and to the coordinated resumption of the cell cycle (Fontanilla and Nuccitelli, 1998; Stricker, 1999; McIsaac et al., 2011; Gelens et al., 2015). Fifteen to twenty minutes after fertilization at 18°C (a common temperature for cultivating *X. laevis*), another wave follows the same path but more slowly. This is the post-fertilization wave (Hara et al., 1977), which coincides with enlargement of the sperm aster (Geertje et al., 1983). Around 70 min after fertilization, a wave emanates from the animal pole, the top of the embryo when oriented with respect to gravity, and travels toward the vegetal pole, the bottom. This is called the first surface contraction wave (Hara et al., 1980; Rankin and Kirschner, 1997). This wave marks the entry of the embryo into mitosis 1, and it is thought to be generated by the interaction of a spherical trigger wave of Cdk1 activation with the cortical cytoskeleton (Chang and Ferrell, 2013). Trigger waves can effectively propagate over large distances, coordinating biological processes along the way (Gelens et al., 2014), and the mitotic wave of Cdk1 activation may serve to synchronize mitotic entry across the fertilized embryo. A second surface contraction wave follows about 10 min later; it also proceeds from the top of the embryo to the bottom and is thought to be due to the interaction of a spherical trigger wave of Cdk1 inactivation with the cortical cytoskeleton (Hara et al., 1980; Rankin and Kirschner, 1997; Chang and Ferrell, 2013). Each of these waves has a suggested role in coordinating developmental processes.

The subsequent cell division waves are perhaps the easiest developmental waves to observe, yet little is known about their origin and biological function. Using time-lapse microscopy and the ability to perturb division timing with temperature, we

This is an open access article under the CC BY-NC-ND license (http://creativecommons.org/licenses/by-nc-nd/4.0/).

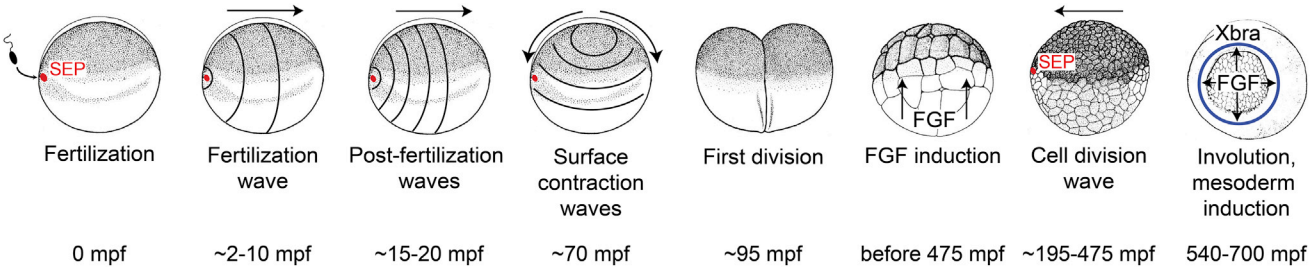

Figure 1. Waves in Early *Xenopus laevis* Development

The *Xenopus laevis* embryo undergoes multiple spatially organized and dynamic events in its early development. Sperm entry point (SEP) denotes the sperm entry point, and mpf is minutes post-fertilization. Adapted from Nieuwkoop and Faber (1994).

sought to understand the role of cell division waves in early embryogenesis. We found that these waves arise through intrinsic differences in cell division timing, surprisingly without an active coupling mechanism. Perturbing the cell division waves resulted in a transient defect in mesoderm induction, which was corrected during involution. This points to the existence of a previously unknown mechanism that corrects problems due to desynchronization prior to gastrulation, thereby contributing to robust embryonic development.

RESULTS

We first set out to quantitatively characterize normal cell division waves in the *X. laevis* embryo. To accomplish this, we observed fertilized embryos in the top view (with the animal pole up and vegetal pole down) using a dissecting microscope and time-lapse video microscopy. We scored individual cell divisions by eye, marking the centroid of the dividing parent cell at the time that the cleavage plane just began to clearly form. We also kept track of the lineages of dividing cells (Movie S3).

As previously shown (Satoh, 1977; Boterenbrood et al., 1983; Newport and Kirschner, 1982a), the first cell cycle is long (~95 min), the subsequent 11 cycles are comparatively short (~35 min), and cell divisions are relatively synchronous within each cycle (Figures 2A–2D). Once many cells were formed, not every division could be scored because some cells were not on the surface of the embryo and others were obscured from view; thus, Figure 2 (as well as the subsequent figures) includes only the subset of divisions that could be scored. Division periods decreased through cell cycle six and then increased beginning at division nine (Figure 2B). A similar trend has been reported in zebrafish (Olivier et al., 2010).

To visualize cell division waves, we needed spatial information about divisions. We plotted the onset of cell divisions as a function of time and cell position. By the time of the fifth cell cycle, waves of cell division were consistently observed. They progressed across the top surface of the embryo toward the sperm entry point (SEP), which usually corresponds to the dorsal-ventral axis (Figure 2C). To visualize several rounds of cell division waves at once, we found it was useful to condense the two-dimensional spatial information into one dimension and plot it against time (Figure 2D). To accomplish this, we projected cell centroids onto a line in the direction of the cell division wave (Movie S3). The wave of cell divisions constituted roughly 10 min out of a 35-min cell cycle period at 18°C (Figures 2C and 2D). This corresponded to an apparent speed of ~2 μm/s.

To characterize the cell division wave in the animal-vegetal direction, which is obscured in the top view, we used optical-quality mirrors mounted on a 45° bias to horizontal in order to observe fertilized embryos from the side (Figure 2E). We found the same trend of decreasing followed by increasing cell cycle period in the side view, but the cell-to-cell period heterogeneity was much greater than in the top view (Figures 2B and 2F). It was difficult to accurately score the first division in this view, so we omit both the first and second periods in Figure 2F. The side view allowed us to observe an orthogonal component of the cell division wave (Movie S2), which again typically became clearly visible around division 5 (Figure 2G). Cells near the bottom, unpigmented vegetal pole divided later than cells near the top, pigmented animal pole, and divisions ran in a smooth wave from top to bottom (Figures 2G and 2H). The cell division wave progressed more slowly along the animal-vegetal axis than along the dorsal-ventral axis, taking up 30 min out of a 35-min cell cycle at 18°C. This corresponded to an apparent speed of 0.7 μm/s.

It has been reported that the first cleavage plane strongly associates with the gray crescent, a feature that in turn forms with respect to the sperm entry point and the post-fertilization wave (Klein, 1987). We verified this, finding a strong correlation between the first cleavage plane axis and the axis of the post-fertilization wave (Figure 2I).

Again, using the origin of the post-fertilization wave as a proxy for sperm entry point location, we found that the cell division wave almost always began on the side opposite the sperm entry point, typically the dorsal side, and terminated near the sperm entry point, typically the ventral side (Figures 2C and 2J). Thus, the post-fertilization wave and the cell division wave travel in opposite directions. This is the reverse of the cell division wave direction described in one early report (Boterenbrood et al., 1983), but it agrees with the findings of Satoh (1977), and it was a consistent finding (Figure 2J).

Does the Cell Division Wave Propagate via Cell-Cell Coupling?

One possible mechanism for the cell division waves is suggested by the discovery that mitosis can propagate through cytoplasm via trigger waves at a speed of ~1 μm/s (Chang and Ferrell, 2013). This mitotic trigger wave propagates from the animal pole to the vegetal pole (Chang and Ferrell, 2013; Pérez-

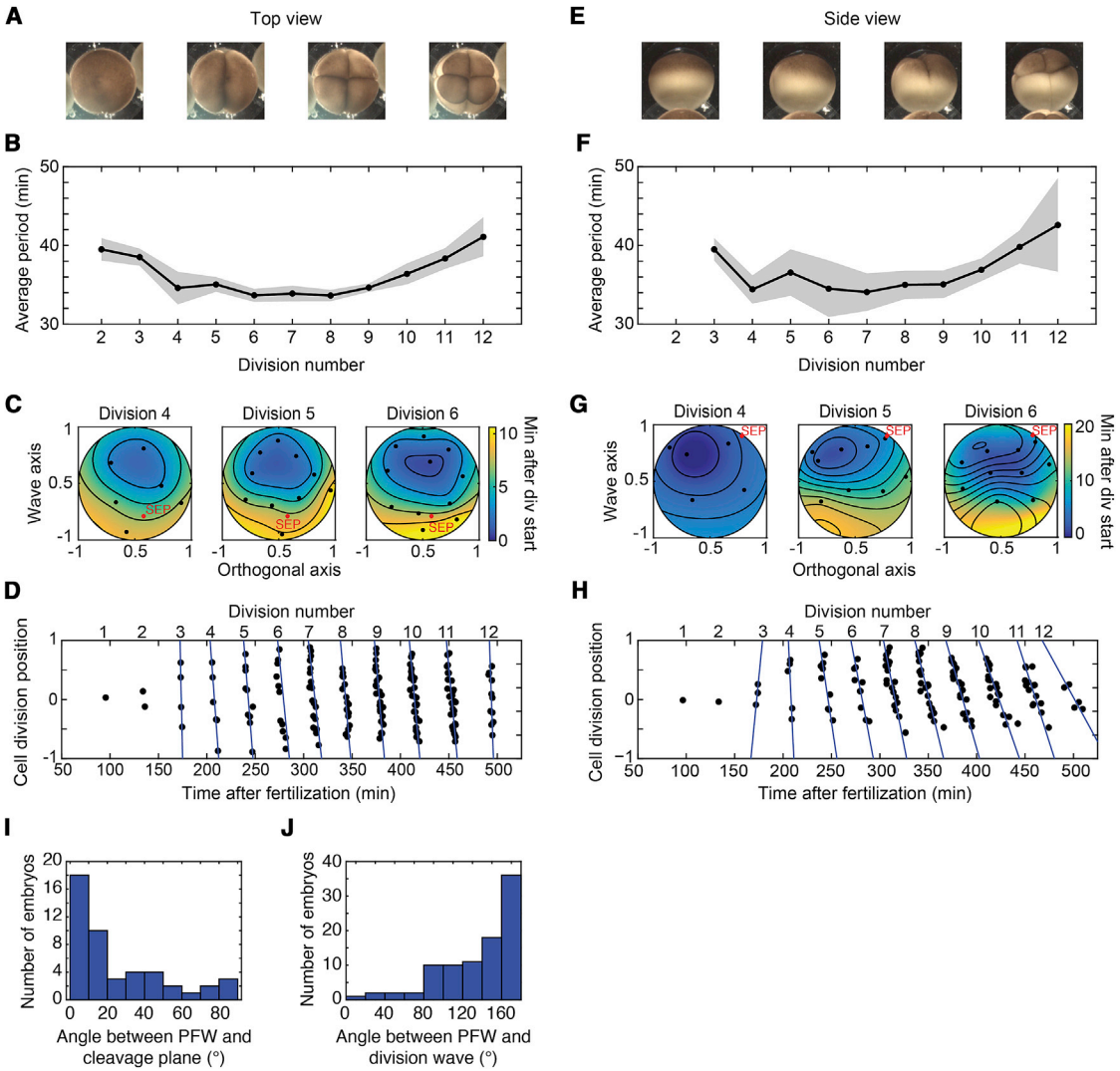

Figure 2. Cell Division Waves in Three Dimensions

The first 12 divisions of the *X. laevis* embryo are regular in time and nearly synchronous within a round of division. Deviations from synchrony take the form of a wave of divisions.

(A) Top view of *X. laevis* embryos at the 1-, 2-, 4-, and 8-cell stage, 18°C.

(B) Cell cycle periods in the top view as a function of time at 18°C. The first cell cycle is much longer and was omitted for clarity. Cell cycle periods shortened slightly through division six and then began lengthening around division 9 or 10, followed by an increase in period at divisions 11 and 12. Error bands are ± one SD.

(C) Top-down view of cell division waves at 18°C. Cell division waves originated opposite the SEP and terminated near the SEP. Color scale denotes the timing of cell division, with cooler colors being earlier divisions. Contours are at two-minute intervals.

(D) Top view of cell division as a function of position and time at 18°C. Lines were fit to rounds of division to illustrate their progression across the surface of the embryo in spatial waves. Centroids of parent cells were projected onto a line that runs along the direction of the division wave and plotted on the y axis.

(E) Side view of *X. laevis* embryos at the 1-, 2-, 4-, and 8-cell stage.

(F) Cell cycle periods in the side view as a function of time at 18°C. The second division is difficult to accurately score in the side view and is omitted along with the first for clarity. Trend of cell cycle periods is similar to the top view in (B) but with more variation. Error bands are ± one SD.

(G) Side view of cell division waves at 18°C. Color scale and contours are as in (C).

(H) Side view of cell division as a function of position and time at 18°C. Centroids of parent cells are projected onto a line that runs along the animal-vegetal axis.

(I) The direction of the first cleavage plane correlates with the direction of the post-fertilization wave.

(J) Cell division waves anti-correlate with the direction of the post-fertilization wave. The post-fertilization wave begins near the sperm entry point and progresses away from it.

The cell division wave begins opposite the SEP and progresses toward it. A total of 47 embryos were analyzed in (I) and 92 in (J).

Mongiovi et al., 1998), similar to the predominantly top-to-bottom direction of the cell division wave. If a mechanism exists for transmitting trigger waves between cells in an embryo, then trigger waves could potentially account for the observed cell division waves.

We therefore set out to test whether cell cycles are coupled in a multicellular embryo. To this end, we elected to transiently delay the division timing of one cell at the two-cell stage. If cell cycles are coupled, the descendants of the delayed and undelayed cells should come back toward synchrony after the delaying perturbation is terminated.

We assessed a number of possible means for creating a delay, and the most suitable proved to be transient application of a temperature gradient. Gradients of temperature have been used in frogs (Huxley, 1927; Black, 1989) and other organisms (Gilchrist, 1928; Niemuth and Wolf, 1995; Jiang et al., 2000; Lucchetta et al., 2005) to preferentially speed up and slow down cell cycles and other developmental phenomena. We reasoned that a temperature gradient would supply the strong but transient change to cell cycle period required to produce a division timing delay.

To this end, we built a device that controls the temperature of two sides of a chamber that is just wide enough to hold a row of *X. laevis* embryos (Figure 3A). Two Peltier-effect heat pumps allowed for the addition or removal of heat from each side of the chamber as necessary to rapidly control a temperature gradient across embryos.

To test the cell-to-cell coupling hypothesis, we applied an 11°C–25°C temperature gradient to embryos from the one-cell stage to the two-cell stage. A 37-min application of this temperature gradient created a ~15-min timing difference between the divisions of the embryo's two cells (Movie S4; Figure 3B). As a control, embryos were placed in the gradient chamber but maintained at a constant temperature of 18°C (Figure 3C).

We then followed the descendants of the transiently warmed cell and of the transiently cooled cell through the next 10 cell divisions. As indicated by the gray regions in Figure 3B, the time between the divisions of the two lineages did not decrease after the temperature gradient was removed. Instead, the average difference in division timing increased slightly as periods increased in the later divisions (Figure 3D). Rather than observing shorter "catching up" periods in the descendants of the cooled cell or longer periods in the descendants of the warmed cell, we saw that average periods in the two lineages were indistinguishable (Figure 3E). Thus, there is no evidence for cell-to-cell coupling; once two cells are out of phase, they remain out of phase indefinitely.

Next, we explored the behavior of embryos that experienced different timing delays to see whether some particular phase differences might be more amenable to resynchronization. As shown in Figure 3F, this was not the case; no matter the initial phase difference, the phase difference was maintained over time and not corrected toward synchrony. Similar results were found when applying the temperature gradient later (after several cell divisions) and/or for longer durations.

Therefore, we have found no evidence for cell-to-cell coupling in creating or maintaining cell division waves. This suggests that cell division waves are instead generated by a cell-autonomous mechanism.

A Simple Model of Cytoplasmic Pre-patterning Can Account for Cell Division Waves

Cell cycle periods in the vegetal half of the embryo were consistently longer than periods in the animal half (Figure 4A), which could be due to differences in yolk content, differences in cyclin mRNA localization (Bowes et al., 2010), or a combination of factors. The period difference was first observable at division four, the first division after the animal and vegetal cytoplasm are separated by cleavage, and was similar in subsequent divisions (Figure 4A). This observation suggested a simple model of autonomous cell division wave generation. In this model, constant differences in cell cycle period that are intrinsic to different parts of the fertilized egg's cytoplasm cause cell division waves to gradually build.

To test whether these period differences alone could give rise to the observed cell division waves, we created a model of the cleaving embryo, making simple assumptions. First, we assumed that period varied linearly throughout the embryo along both the animal-vegetal axis and the dorsal-ventral axis. Then, we assumed that cells respond to the local period at their midpoint. The alternate assumption, that cells respond to an average period over their volume, yielded similar results. Finally, we let the model segment a cubic volume similarly to how cells in the *X. laevis* embryo divide (Figure 4B) and calculated the period in each of the daughter cells. The cubic geometry is of course an approximation but was sufficient to capture the essence of the partitioning process. The model produced waves of divisions that appeared remarkably similar to experimentally measured divisions in the top view and side view (Figures 4C and 4F). The best match to experimentally observed cell division waves was obtained by assuming that the period intrinsic to the fastest part of the embryo was 18% shorter than the period in the slowest part (Figure S1A). This corresponded to a predicted period difference of three minutes at the hemisphere midpoints, similar to measured period differences for cycles 4, 5, and 6 (Figures S1B and S1C). Therefore, the development of cell division waves could occur through the gradual and steady accumulation of timing differences pre-patterned in the fertilized egg.

Developmental Consequences of Asynchronous MBT Entry

The lack of evidence for coupling in the cell division wave led us to wonder whether the timing of early embryonic cell divisions is important for subsequent developmental events. As mesoderm is specified during these early rounds of cell division, we tested whether the normal near-synchronous divisions were necessary for proper mesoderm induction. To this end, we subjected embryos to a sustained 11°C–25°C temperature gradient orthogonal to the animal-vegetal axis (side to side) or along the animal-vegetal axis (top to bottom), from the one-cell stage to the time just before the first cells entered the midblastula transition (7 or 8 hr post-fertilization [hpf]; Nieuwkoop and Faber [NF] stage 9). This resulted in embryos with drastic timing differences between the warmed and cooled sides and drastically different sizes of cells: large cells that had completed fewer divisions on the cooled side and small cells that had completed more divisions on the warmed side (Figure 5A; Movies S5, S6, S7, S8, S9, and S10).

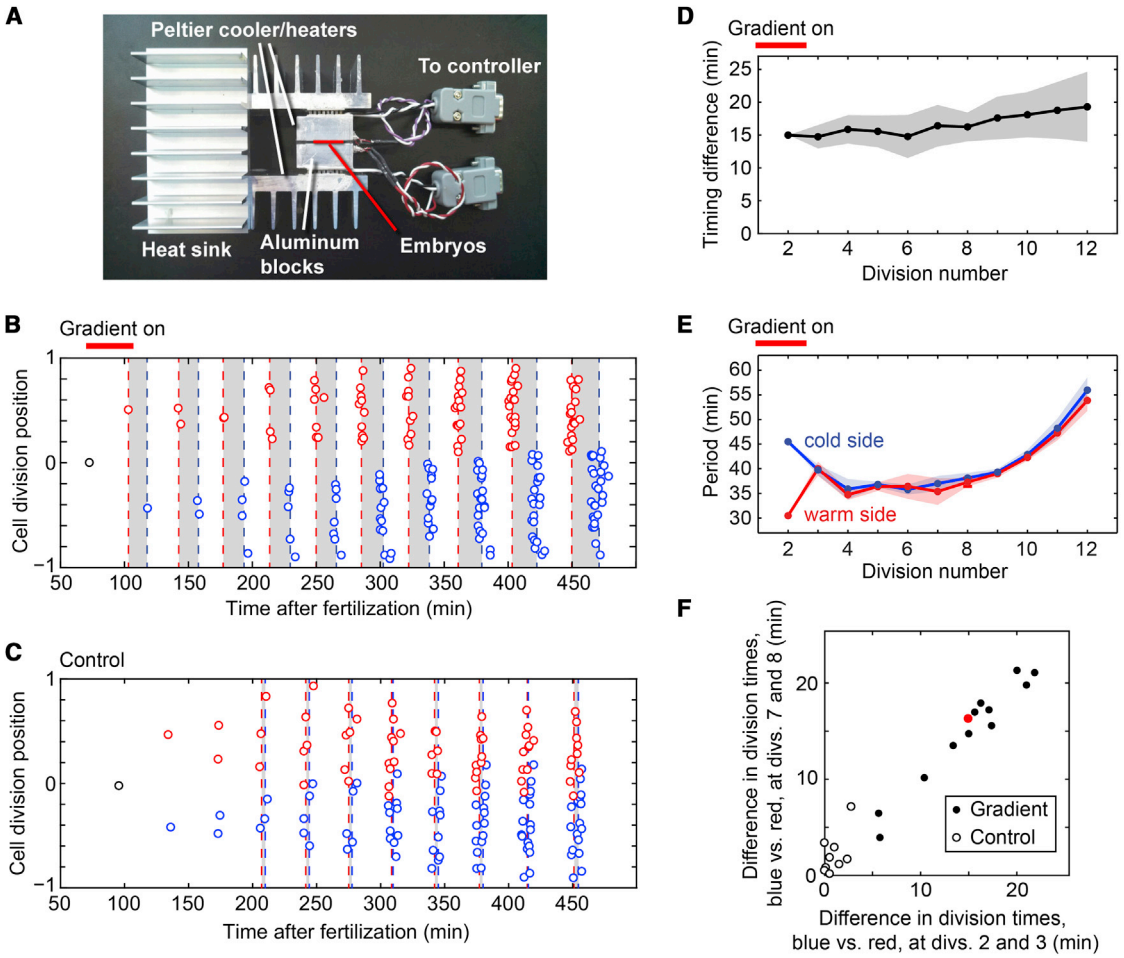

Figure 3. A Temperature Gradient Reveals Lack of Coupling in Cell Divisions

(A) Temperature gradient device.

(B) Desynchronizing cell divisions. Embryo was initially maintained at 23°C and then a temperature gradient of 11°C–25°C was applied during the time marked by the horizontal red bar, from 70 mpf to 107 mpf. The second round of cell divisions was desynchronized as a result, with the two divisions occurring approximately 15 min apart. Temperature was then uniformly set to 18°C for the remainder of time. Subsequent divisions were labeled red (descendants of the warmed cell) and blue (descendants of the cooled cell). Vertical lines indicate average division time of each group, and gray regions indicate the difference in average division time between the groups.

(C) Cell divisions in a mock-treated control embryo at 18°C.

(D) The difference in average division time between descendants of cooled cells and descendants of warmed cells. These values correspond to the width of gray regions in (B). The error band is ±1 SD of the timing difference.

(E) Average periods in lineages descended from the cooled cell (blue) and warmed cell (red) at the two-cell stage. Error bands are ±1 SD of the period.

(F) Comparison of early- and late-division timing. Average timing differences measured at divisions two and three were compared with average timing differences measured at divisions seven and eight. For gradient embryos, timing differences were between descendants of warmed and cooled cells, and the temperature gradient was applied with different durations, ranging from 37 to 57 min (always starting at 70 mpf). For control embryos, timing differences were between descendants of the two-cell stage. Red point is the embryo in (B), (D), and (E).

In order to estimate the timing of the midblastula transition (MBT) in embryos that were held at fixed temperature but previously experienced a side-to-side gradient (Figure 5), we kept track of cell divisions in a selected region on the previously hot side (smaller cells) and the previously cold side (larger cells). We then used this to determine the number of visible cells in those regions (Figure 5B) and analyzed the corresponding average rate of cell division in each region. This division rate initially increased as more dividing cells accumulate inside the region but then started to decrease as cells entered MBT, which was accompanied by much slower cell divisions (Figure 5C). Moreover, the onset of MBT was also characterized by an increased motility of the cells (Movie S6). This analysis shows that cells on the previously cold side entered MBT ~60 min (SD: 16 min; n = 3) later than cells on the previously hot side, a time difference that corresponds to about two full cycles. Figure 5 thus argues that all cells that were slowed down due to the cooling continue to divide until they have finished the same number of divisions as the fast, warmed cells had.

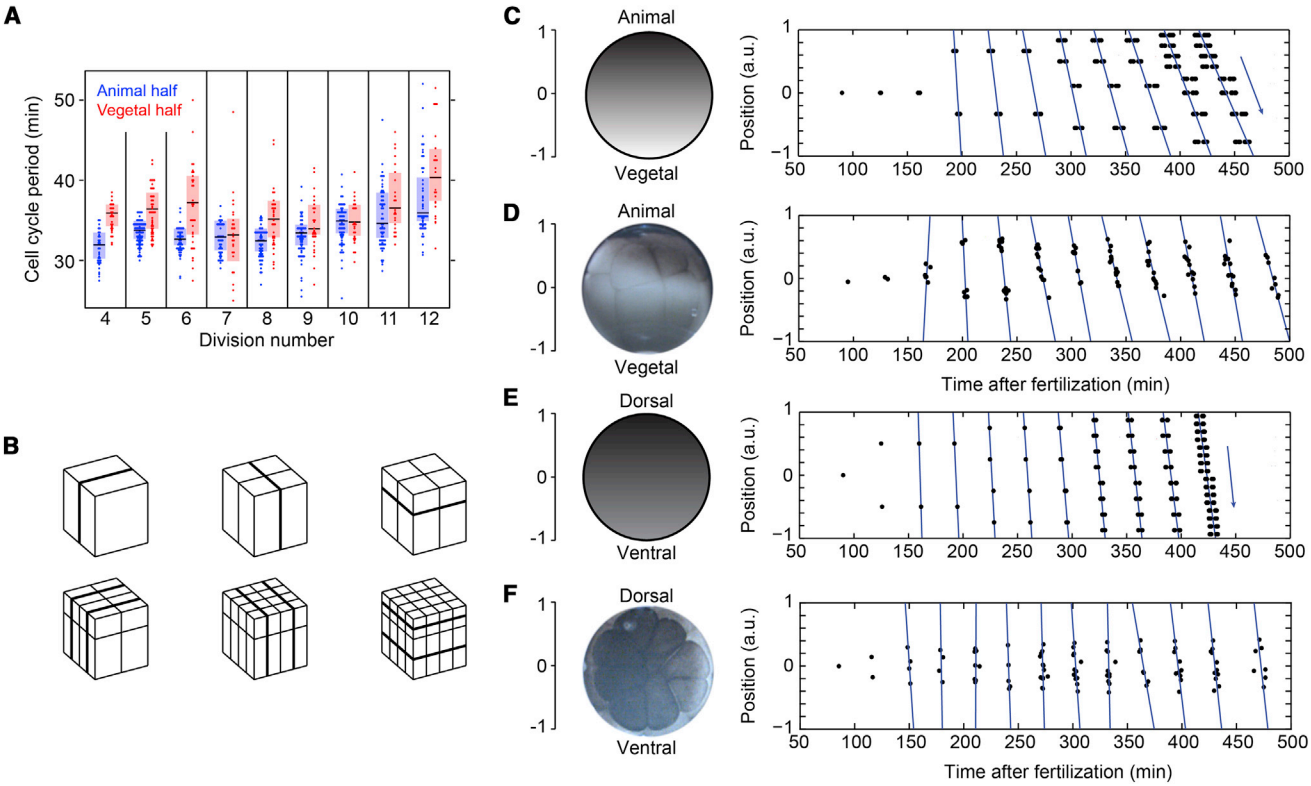

Figure 4. A Simple Model Accounts for Cell Division Waves

(A) Cell-cycle periods for cells in the animal half (blue) and vegetal half (red) of nine unperturbed embryos at 18°C. Black bars are medians, and the shaded boxes indicate 25th and 75th percentiles.

(B) The first six simulated divisions of a cubic space representing the embryo.

(C–F) Simulated cell division waves in the side view (C) and top view (E). (D) and (F) are experimentally measured cell division waves at 18°C for comparison. See also Figure S1.

After the onset of MBT, mesoderm induction can be evaluated by in situ hybridization for the mesodermal marker *Xbra*. In control embryos, *Xbra* expression was absent at 8 hpf, but a faint symmetrical ring of *Xbra* expression could be seen as soon as 8:15 hpf (Figure S2A). This ring of *Xbra* expression became stronger and thicker in the following hours (measured at 8:30 hpf, 9:30 hpf, 10 hpf, and 12 hpf) but always maintained its characteristic symmetric ring shape (Figures 6A, S2A, and S2B). In contrast, in the embryos desynchronized with a side-to-side temperature gradient (Figure S2C; Movie S5), *Xbra* was expressed in a highly asymmetrical arc (Figures 6A, S2B, and S2E). The arc coincided spatially with the concentration of pigmented bottle cells and the slight lip that marks the blastopore at the beginning of involution (Hardin and Keller, 1988; Black, 1989; Nieuwkoop and Faber, 1994; Keller, 1981). Pigmented bottle cells, in turn, appear first on the previously heated side of temperature-gradient-treated embryos (Movie S7), linking the orientation of the temperature gradient with the orientation of the arc of *Xbra* expression. These findings suggest that disrupting the endogenous early cell division timing using a temperature gradient, which leads to an asynchronous entry into MBT, affects the organization of the mesoderm during gastrulation.

After observing this effect of a side-to-side temperature gradient, we wondered whether a temperature gradient in a different direction might produce different effects. We rotated the gradient device 90° and applied a temperature gradient along the animal-vegetal axis (the top-to-bottom direction) of embryos from the first cell cycle to just before MBT. 45-degree mirrors allowed us to visualize embryonic development during this top-to-bottom gradient. We warmed the vegetal pole and chilled the animal pole in order to reverse the normal animal-vegetal component of the cell division wave (Figure S2D; Movie S8). As shown in Figure 6A, *Xbra* was expressed normally and symmetrically in embryos that experienced a top-to-bottom temperature gradient (see also Figure S2B). Therefore, the observed asymmetric *Xbra* pattern in side-to-side gradient experiments was not due simply to the presence or creation of the temperature gradient itself. Instead, this *Xbra* pattern resulted from the application of a temperature gradient specifically along axes orthogonal to the animal-vegetal axis.

Consequences of Asynchrony for Embryonic Survival

Finally, we asked whether embryos would survive to develop into normal tadpoles following highly asynchronous MBT entry and mesoderm induction. We performed the side-to-side and top-to-bottom gradient treatments as previously described and then removed embryos from the gradient chamber and

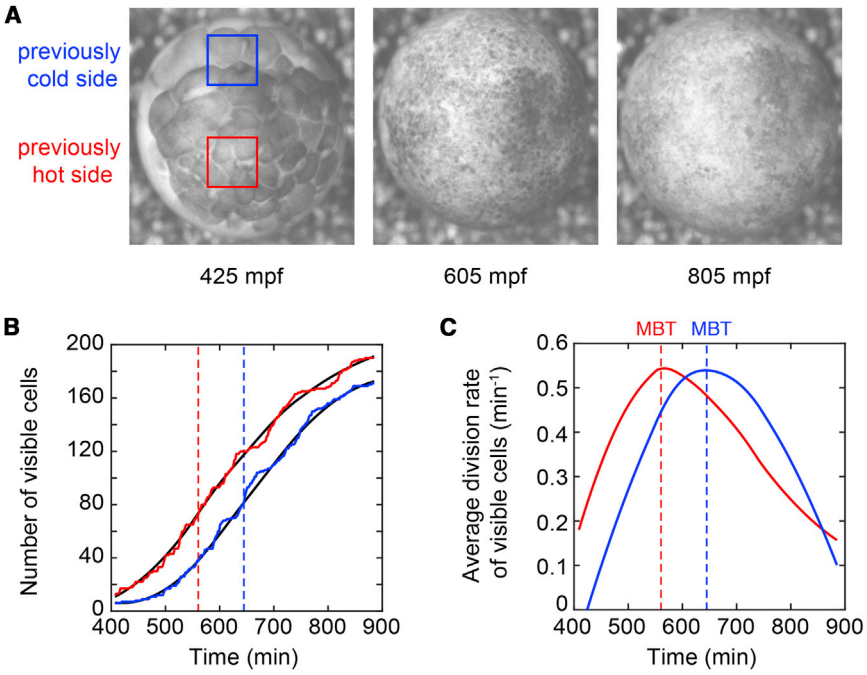

Figure 5. A Side-to-Side Temperature Gradient Leads to Asynchronous MBT Entry

(A) Snapshots of embryo at 23°C at three different time points after it has experienced a side-to-side temperature gradient (11°C–25°C) from 1:10 hpf to 5:45 hpf. Two regions of equal size have been selected on the previously cold and previously warm side.

(B) Number of visible cells in the previously cold region (blue) and the previously warm region (red) as indicated in (A). The number of visible cells has been calculated by taking the initial number of cells and then increasing it by one every time a cell division is observed. The black lines show a smoothed fit using the "robust LOESS" (quadratic fit) option in MATLAB.

(C) The average division rate of the visible cells as calculated from the fitted curves in (B). The time of maximal average division rate is taken as a measure for MBT onset. MBT is found to occur ~60 min later in the previously cold region than in the previously warm region (with a SD of 16 min; 3 analyzed embryos).

observed their development for two weeks. Remarkably, despite the *Xbra* misexpression that resulted from the side-to-side gradient, we found no significant difference between the rate of survival with generally normal phenotype for embryos that experienced a gradient and those that were simply placed in a gradient chamber at uniform 18°C for the same amount of time (Movies S9 and S10; Figures 6B and 6C). These results are consistent with the findings of Black (1989) and Huxley (1927), where it was reported that temperature gradients can change the orientation of the dorsal lip but do not reset the dorsal-ventral axis.

To determine how the gradient-treated embryos were able to recover from their aberrant *Xbra* expression pattern, we repeated the gradient treatment and examined *Xbra* staining at times later in development to see what became of the misexpressed pattern. By 12 hpf, gradient-treated embryos expressed a symmetric ring of *Xbra* around their vegetal pole, just like control embryos at 10 hpf. Following this time point, gradient-treated embryos seemed to display normal but delayed *Xbra* expression, performing normal neurulation and expressing *Xbra* in a characteristic shape (Figure 6A). Strikingly, the *Xbra* expression defect in embryos that entered MBT asynchronously was corrected by 12 hpf, NF stage 10.5. This recovery of a normal *Xbra* expression pattern after a side-to-side temperature gradient suggests the existence of a corrective process that is carried out at approximately the time of involution. The corrective process is able to take thousands of autonomously dividing cells and coordinate them to express a symmetric ring of *Xbra*.

DISCUSSION

Newport and Kirschner (1982a) showed that *X. laevis* embryonic cells continue to divide with near-normal periods when dissociated from their embryonic context. This implied that each cell possesses an independent and accurate cell cycle clock, yet the result left open the possibility that, in the intact embryo, cells are coupled to actively maintain near-synchrony of cell division timing in the face of perturbation.

Here, we found that *X. laevis* embryos do not rely on cell-to-cell coupling to maintain cell division timing. Transiently desynchronized embryos fail to become more synchronous and instead remain desynchronized, dividing in an autonomous and apparently uncoupled manner. Thus, we ruled out mechanisms for producing a cell division wave that rely on a trigger wave or intercellular coupling.

The cell cycle period is shortest in the animal half and longest in the vegetal half. This period difference could be accounted for by the heterogeneous distribution of cyclin B1 and cyclin B2 mRNA, with greatest concentration in the animal hemisphere (Bowes et al., 2010). Similarly, the yolk material is strongly concentrated in the vegetal hemisphere. Additionally, it has been shown that animal yolk material (and perhaps period determinants) is also rearranged during the first cell cycle as a result of the growing sperm aster (Ubbels et al., 1983; Brown et al., 1993; Kikkawa et al., 1996). Likewise, cell division waves begin near the animal pole and terminate near the vegetal pole. An orthogonal component of division waves travels from opposite the sperm entry point toward the sperm entry point. These waves develop gradually over multiple cell cycles into smooth patterns of division, and a model that assumes autonomous divisions and linearly varying cell cycle periods recapitulates the waves and their evolution.

Despite the lack of active coordination in early embryonic cell division timing, normal near-synchrony is required for the proper initiation of mesoderm induction, as read out by the transcription factor *Xbra*. Similarly, the timing of MBT was found to be strongly

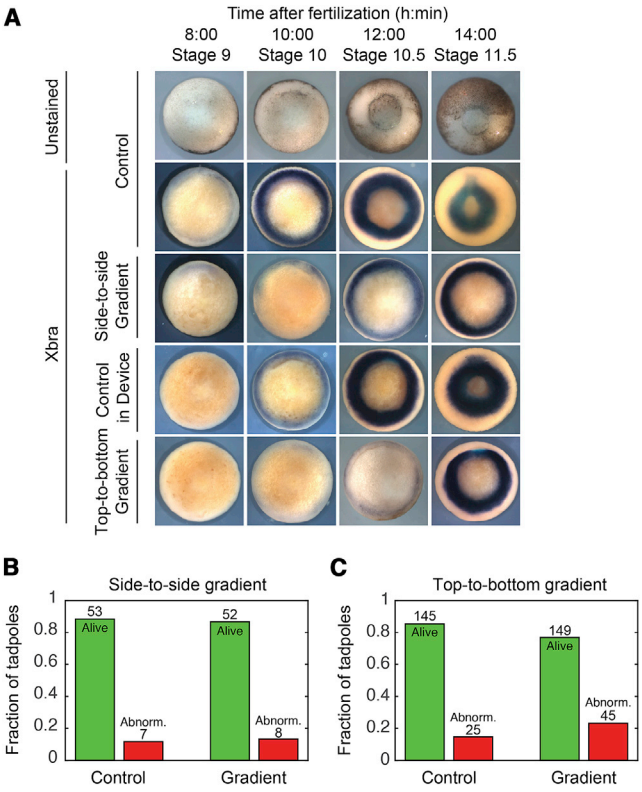

Figure 6. A Long Temperature Gradient Induces a Mesodermal Induction Defect and Reveals a Resynchronizing Mechanism

(A) *Xbra* expression after MBT. Time course of *Xbra* expression in gradient embryos treated in the side to side and top to bottom directions. Unstained and mock-treated control embryos are shown for comparison.

(B and C) Phenotype and survival of embryos two weeks after treatment with a side-to-side (B) or top-to-bottom (C) gradient. "Alive" includes embryos that survived with a generally normal phenotype, and "abnormal" includes embryos that did not survive and embryos that experienced clear developmental defects, such as dorsalization, ventralization, and bent body axes.

asynchronous, which points to a relationship between cell size and the onset of MBT and cell differentiation, as also suggested before (Newport and Kirschner 1982b; Farrell and O'Farrell 2014; Amodeo et al., 2015). However, near-synchrony along the animal-vegetal axis is not required for proper *Xbra* patterning, which suggests that the observed mesodermal patterning defect is only caused by the developmental delay induced by the side-to-side temperature gradient.

Remarkably, asynchrony-induced *Xbra* misexpression was corrected during involution, resulting in a delayed but otherwise normal, spatially symmetric *Xbra* pattern. Embryos recovered from asynchrony with generally normal development and normal survival rates. Perhaps this secondary resynchronization during involution explains why, unlike other waves in the early embryo, the cell division wave lacks active regulation.

Thus, the *X. laevis* embryo displays extreme robustness to environmental perturbation. It uses simple mechanisms to prepare a fertilized zygote for the complex rearrangements of gastrulation. *Drosophila* and the wasp *Pimpla turionellae* also possess robustness to temperature gradient perturbation, developing normally after desynchronization of embryonic cell lineages (Lucchetta et al., 2005; Niemuth and Wolf, 1995).

Why are embryos built to survive perturbations to division timing they would likely never encounter in nature? Are these perturbations simply more extreme versions of the cell division asynchrony embryos are already selected to tolerate? (Cells along the animal-vegetal axis of an unperturbed *X. laevis* embryo enter MBT over a window of 30 min at 18°C, for example.) Or is robustness to asynchrony an exaptation—a beneficial trait that evolved in response to an unrelated need, perhaps the need to globally coordinate cell lineages during involution?

Although we have identified the approximate moment when resynchronization occurs, the mechanism remains elusive. One intriguing idea is that, after MBT, there exists some unknown checkpoint that pauses differentiation and further development until all cells have reached the same required status. Such a checkpoint that ensures symmetrical morphogenesis might have had a high priority in fitness during evolution. Making precise measurement of cell cycle periods after MBT but before involution, paying special attention to abnormally short or long periods in gradient-treated embryos, could help to answer this question.

The rounds of cell cleavage following fertilization of the *X. laevis* embryo have surprised us with their minimal complexity. Because this period of development prepares the embryo for the complex rearrangements of gastrulation, we initially expected the timing of cell division waves to be highly regulated. We have instead come to expect elegant robustness from the early embryo.

EXPERIMENTAL PROCEDURES

Embryos

Xenopus laevis adult females were primed with 67 IU of pregnant mare serum gonadotropin at least 3 days prior to induction and induced with 500 IU of human chorionic gonadotropin 16 hr prior to ovulation. Eggs were squeezed from ovulating females and fertilized using dissected testes and then dejellied by gently swirling a dish of embryos in 2% cysteine (pH 7.8). After 3 or 4 min in cysteine, fertilized embryos were washed ~10× in 0.1× Marc's modified Ringer's solution (MMR) (Murray, 1991). Development was observed in 0.1× MMR.

Time-Lapse Microscopy

Throughout this study, we collected data by time-lapse microscopy on a dissection microscope with a 0.5× objective and a variable zoom. An attached camera recorded images for later analysis. We used frame rates of once every 10 s and once every 30 s.

Mirrors

Fertilized and dejellied *X. laevis* embryos orient with respect to gravity such that one can image only their gravity-up animal pole with a standard dissecting microscope. To examine the sides and the gravity-down vegetal pole of the embryo, we made use of an optical-quality mirror manufactured to sit at 45 degrees from horizontal, the half-cube 4.2-mm mirror from Edmund Optics. These mirrors were placed near an embryo and reflected light 90 degrees upward to a dissecting microscope. Placing an embryo between two such mirrors allowed us to view two sides of a single embryo. With this setup, we were able to record a majority of embryonic surface divisions.

Mirror Imaging Chamber

We used the large temperature-controlled chamber described in Gelens et al. (2015) to observe unperturbed embryos from the top down and in the side view using 45-degree mirrors.

Timing of Divisions within an Embryo

Because *X. laevis* embryos are opaque, we could not use fluorescence-based markers to visualize cell divisions. Instead, we scored bright field movies for the timing and position of cell divisions by eye. To assist in the task, we developed custom software using MATLAB to record scored division information. Our software allows replay of a movie frame by frame so the user can carefully identify divisions. We scored division time as the first frame during which any part of the dark cleavage plane is clearly visible, and we scored division location as the centroid of the visible portion of a dividing parent cell. Both time and position information are recorded with a click and then the user scrolls backward in time to find the parent of the scored cell. In this way, the user works backward division by division to either the first frame of the movie or to a previously scored parent. The software then adds the recently scored lineage to a tree of cell relationships within the embryo.

Temperature Gradient Device

The temperature gradient device is composed of a chamber, temperature-controlling machinery, and aluminum heat sinks. The chamber is formed by a Lexan insert sandwiched between two aluminum blocks. Each block contains an internal thermistor to monitor its temperature. A Peltier cooler/heater is glued to the outside edge of each aluminum block with thermally conductive glue, and aluminum heat sinks attach to the Peltier devices. The thermistors and Peltier devices are linked to a digital temperature controller, which allows us to precisely (within 0.1°C) and independently control the temperature of each aluminum block. A row of embryos rests on the Lexan insert between the two aluminum blocks and is covered from above with a glass coverslip sealed with a mixture of equal masses melted petroleum jelly:lanolin:paraffin wax (VLP). For side-to-side gradients in the direction orthogonal to the animal-vegetal axis, the chamber is filled with 0.5% low-melting-point agarose in 0.1× MMR to prevent convection from influencing the development of a linear temperature gradient. In top-to-bottom gradients along the animal-vegetal axis, the chamber was filled with 0.1× MMR and no agarose to allow embryo reorientation, but the gradient device still produced comparable timing differences.

To prepare embryos for a gradient experiment, we fertilized them, removed their jelly coats (Murray, 1991), and placed them in the gradient device's chamber along with 0.1× MMR. If adding agarose, we removed the MMR to a level just above the embryos and then added 0.5% low-melting-point agarose dissolved in 0.1× MMR, previously held at 36°C, to fill the chamber. We maintained embryos at a uniform and constant 23°C while filling the chamber with warm agarose.

The Short-Gradient Experiment

Next, we needed to pick appropriate times to apply the temperature gradient with the goal of creating a large difference in timing between adjacent cells while still leaving plenty of time remaining to observe divisions after gradient termination. To satisfy these requirements, we applied temperature gradients at the one- and two-cell stages, terminating in time to observe the third division onward at uniform temperature.

Fertilization and dejellying were carried out at room temperature. Accordingly, embryos were maintained at 23°C before beginning the gradient. During the gradient, we used a variety of temperatures that spanned a range including the highest and lowest temperatures that embryos could tolerate, 11°C–25°C. Gradients were applied before the first division, typically at 70 mpf, and were terminated before the second division was complete, typically at 1:47 hpf. The gradient device required about a minute to come to a new temperature after being set. For example, it took 73 s to chill one block to 9°C while maintaining the other at 23°C.

After gradient termination, there is a challenge in temperature selection. Too cold and the remaining divisions take days to complete. Too hot and experimental and scoring noise obscures division timing. We compromised and brought embryos to a uniform 18°C after terminating the gradient.

The Long-Gradient Experiment

For long gradient experiments, we prepared embryos identically to the short gradient and then simply waited to terminate the gradient until division number 10. In these experiments, we removed embryos from the chamber immediately after gradient termination and observed their development in a dish filled with 0.1× MMR and then either fixed at time points for in situ staining or transferred to 24-well plates filled with 0.1× MMR for long-term survival and phenotype observation.

Because of the gravity orientation of fertilized *X. laevis* embryos, our gradient device typically applies a temperature gradient along an axis orthogonal to gravity. To apply the gradient along the axis of gravity, we simply sealed fertilized dejellied embryos in the gradient chamber, without removing MMR or adding agarose, and then turned the gradient device 90° so that one aluminum block faced down and the other faced up. The embryos reoriented with respect to gravity, so their bottom vegetal pole was in contact with one aluminum block and their top animal pole was in contact with the other. We then placed 45° mirrors outside the chamber such that they directed light emanating horizontally from the chamber upward into the microscope.

RNA In Situ Hybridization

Staining was performed as in Harland (1991).

Regulatory Approval

All experiments on live vertebrates were performed in accordance with relevant institutional and national guidelines and regulations; the Stanford University Administrative Panel on Laboratory and Animal Care approved the experiments.

SUPPLEMENTAL INFORMATION

Supplemental Information includes Supplemental Experimental Procedures, two figures, and ten movies and can be found with this article online at https://doi.org/10.1016/j.celrep.2017.09.017.

AUTHOR CONTRIBUTIONS

G.A.A., L.G., J.C.B., and J.E.F. designed the studies; G.A.A. and L.G. carried out the experiments and the modeling; and G.A.A., L.G., J.C.B., and J.E.F. wrote the paper.

ACKNOWLEDGMENTS

We would like to thank Jessica Chang for in situ instruction and sharing her bench; Tek Hyung Lee, Sarah Trosin, and Julia Kamenz for comments; and all the members of the Baker and Ferrell labs for comments, advice, and being wonderful people to work with. L.G. thanks Guy Verschaffelt and Lars Keuninckx of the Applied Physics Group for their help with the initial design of the gradient embryo chamber. This work was supported in part by grants from the NIH (R01 GM110564 and P50 GM107615 to J.E.F. and R01 GM103787 and R01 HD076839 to J.C.B.); the National Science Foundation Graduate Research Fellowship Program to G.A.A.; and the Research Foundation-Flanders (FWO-Vlaanderen), the Belgian American Educational Foundation (BAEF), the KU Leuven Junior Mobility Programme (JuMO), and the Research Council of the Vrije Universiteit Brussel to L.G.

Received: July 6, 2016
Revised: July 20, 2017
Accepted: September 4, 2017
Published: October 3, 2017

REFERENCES

Amodeo, A.A., Jukam, D., Straight, A.F., and Skotheim, J.M. (2015). Histone titration against the genome sets the DNA-to-cytoplasm threshold for the Xenopus midblastula transition. Proc. Natl. Acad. Sci. U.S.A. *112*, E0186–E1095.

Black, S.D. (1989). Experimental reversal of the normal dorsal-ventral timing of blastopore formation does not reverse axis polarity in *Xenopus laevis* embryos. Dev. Biol. *134*, 376–381.

Boterenbrood, E.C., Narraway, J.M., and Hara, K. (1983). Duration of cleavage cycles and asymmetry in the direction of cleavage waves prior to gastrulation in *Xenopus laevis*. Wilehm Roux Arch Dev Biol *192*, 216–221.

Bowes, J.B., Snyder, K.A., Segerdell, E., Jarabek, C.J., Azam, K., Zorn, A.M., and Vize, P.D. (2010). Xenbase: gene expression and improved integration. Nucleic Acids Res. *38*, D607–D612.

Brown, E.E., Denegre, J.M., and Danilchik, M.V. (1993). Deep cytoplasmic rearrangements in ventralized *Xenopus* embryos. Dev. Biol. *160*, 148–156.

Chang, J.B., and Ferrell, J.E., Jr. (2013). Mitotic trigger waves and the spatial coordination of the *Xenopus* cell cycle. Nature *500*, 603–607.

Farrell, J.A., and O'Farrell, P.H. (2014). From egg to gastrula: how the cell cycle is remodeled during the Drosophila mid-blastula transition. Annu. Rev. Genet. *48*, 69–94.

Fontanilla, R.A., and Nuccitelli, R. (1998). Characterization of the sperm-induced calcium wave in Xenopus eggs using confocal microscopy. Biophys. J. *75*, 2079–2087.

Geertje, U.A., Hara, K., Koster, C.H., and Kirschner, M.W. (1983). Evidence for a functional role of the cytoskeleton in determination of the dorsoventral axis in Xenopus laevis eggs. J. Embryol. Exp. Morph. *77*, 15–37.

Gelens, L., Anderson, G.A., and Ferrell, J.E., Jr. (2014). Spatial trigger waves: positive feedback gets you a long way. Mol. Biol. Cell *25*, 3486–3493.

Gelens, L., Huang, K.C., and Ferrell, J.E., Jr. (2015). How does the *Xenopus laevis* embryonic cell cycle avoid spatial chaos? Cell Rep. *12*, 892–900.

Gilchrist, F.G. (1928). The effect of a horizontal temperature gradient on the development of the egg of the Urodele, Triturus torosus. Physiol. Zool. *1*, 231–268.

Hara, K., Tydeman, P., and Hengst, R.T.M. (1977). Cinematographic observation of "post-fertilization waves" (PFW) on the zygote of*Xenopus laevis*. Wilehm Roux Arch Dev Biol *181*, 189–192.

Hara, K., Tydeman, P., and Kirschner, M. (1980). A cytoplasmic clock with the same period as the division cycle in *Xenopus* eggs. Proc. Natl. Acad. Sci. USA *77*, 462–466.

Hardin, J., and Keller, R. (1988). The behaviour and function of bottle cells during gastrulation of Xenopus laevis. Development *103*, 211–230.

Harland, R.M. (1991). In situ hybridization: an improved whole-mount method for *Xenopus* embryos. Methods Cell Biol. *36*, 685–695.

Huxley, J.S. (1927). The modification of development by means of temperature gradients. Wilhelm Roux'. Arch. Entwickl. Mech. Org. *112*, 480–516.

Jiang, Y.J., Aerne, B.L., Smithers, L., Haddon, C., Ish-Horowicz, D., and Lewis, J. (2000). Notch signalling and the synchronization of the somite segmentation clock. Nature *408*, 475–479.

Keller, R.E. (1981). An experimental analysis of the role of bottle cells and the deep marginal zone in gastrulation of *Xenopus laevis*. J. Exp. Zool. *216*, 81–101.

Keller, P.J., Schmidt, A.D., Wittbrodt, J., and Stelzer, E.H.K. (2008). Reconstruction of zebrafish early embryonic development by scanned light sheet microscopy. Science *322*, 1065–1069.

Kikkawa, M., Takano, K., and Shinagawa, A. (1996). Location and behavior of dorsal determinants during first cell cycle in *Xenopus* eggs. Development *122*, 3687–3696.

Klein, S.L. (1987). The first cleavage furrow demarcates the dorsal-ventral axis in *Xenopus* embryos. Dev. Biol. *120*, 299–304.

Lucchetta, E.M., Lee, J.H., Fu, L.A., Patel, N.H., and Ismagilov, R.F. (2005). Dynamics of *Drosophila* embryonic patterning network perturbed in space and time using microfluidics. Nature *434*, 1134–1138.

McIsaac, R.S., Huang, K.C., Sengupta, A., and Wingreen, N.S. (2011). Does the potential for chaos constrain the embryonic cell-cycle oscillator? PLoS Comput. Biol. *7*, e1002109.

Murray, A.W. (1991). Cell cycle extracts. Methods Cell Biol. *36*, 581–605.

Newport, J., and Kirschner, M. (1982a). A major developmental transition in early *Xenopus* embryos: I. characterization and timing of cellular changes at the midblastula stage. Cell *30*, 675–686.

Newport, J., and Kirschner, M. (1982b). A major developmental transition in early Xenopus embryos: II. Control of the onset of transcription. Cell *30*, 687–696.

Niemuth, J., and Wolf, R. (1995). Developmental asynchrony caused by steep temperature gradients does not impair pattern formation in the wasp, Pimpla turionellae L. Rouxs Arch. Dev. Biol. *204*, 444–452.

Nieuwkoop, P.D., and Faber, J. (1994). Normal Table of *Xenopus laevis* (Daudin) (New York: Garland Publishing).

Olivier, N., Luengo-Oroz, M.A., Duloquin, L., Faure, E., Savy, T., Veilleux, I., Solinas, X., Débarre, D., Bourgine, P., Santos, A., et al. (2010). Cell lineage reconstruction of early zebrafish embryos using label-free nonlinear microscopy. Science *329*, 967–971.

Pérez-Mongiovi, D., Chang, P., and Houliston, E. (1998). A propagated wave of MPF activation accompanies surface contraction waves at first mitosis in *Xenopus*. J. Cell Sci. *111*, 385–393.

Rankin, S., and Kirschner, M.W. (1997). The surface contraction waves of *Xenopus* eggs reflect the metachronous cell-cycle state of the cytoplasm. Curr. Biol. *7*, 451–454.

Satoh, N. (1977). 'Metachronous' cleavage and initiation of gastrulation in amphibian embryos. Dev. Growth Differ. *19*, 111–117.

Stricker, S.A. (1999). Comparative biology of calcium signaling during fertilization and egg activation in animals. Dev. Biol. *211*, 157–176.

Tomer, R., Khairy, K., Amat, F., and Keller, P.J. (2012). Quantitative high-speed imaging of entire developing embryos with simultaneous multiview light-sheet microscopy. Nat. Methods *9*, 755–763.

Ubbels, G.A., Hara, K., Koster, C.H., and Kirschner, M.W. (1983). Evidence for a functional role of the cytoskeleton in determination of the dorsoventral axis in *Xenopus laevis* eggs. J. Embryol. Exp. Morphol. *77*, 15–37.